Cancer Letters 460 (2019) 42–53

Contents lists available at ScienceDirect

Cancer Letters

journal homepage: www.elsevier.com/locate/canlet

Original Articles

Cell-intrinsic PD-1 promotes proliferation in pancreatic cancer by targeting CYR61/CTGF via the hippo pathway

Ning Pu[a,c,1], Shanshan Gao[b,1], Hanlin Yin[a,1], Jian-ang Li[a], Wenchuan Wu[a], Yuan Fang[a], Lei Zhang[a], Yefei Rong[a], Xuefeng Xu[a], Dansong Wang[a], Tiantao Kuang[a], Dayong Jin[a], Jun Yu[c,*], Wenhui Lou[a,**]

[a] Department of General Surgery, Zhongshan Hospital, Fudan University, Shanghai, 200032, China
[b] Department of Interventional Radiology, Zhongshan Hospital, Fudan University, Shanghai, 200032, China
[c] Department of Surgery, The Sol Goldman Pancreatic Cancer Research Center, The Johns Hopkins University School of Medicine, Baltimore, MD, 21287, USA

ARTICLE INFO

Keywords:
Pancreatic ductal adenocarcinoma
Programmed cell death protein-1
Immune checkpoint
Hippo signaling
Nomogram

ABSTRACT

Pancreatic ductal adenocarcinoma (PDAC) remains a refractory disease. Programmed cell death protein-1 (PD-1) monotherapy has shown strong performance in targeting several malignancies. However, the effect and mechanism of intrinsic PD-1 in pancreatic cancer cells is still unknown. In this study, associations between clinicopathological characteristics and stained tissue microarrays of PDAC specimens were analyzed along with profiling and functional analyses. The results showed that cell-intrinsic PD-1 was significantly correlated with overall survival (OS). Independently of adaptive immunity, intrinsic PD-1 promoted tumor growth in PDAC. Concomitantly, the overexpression of intrinsic PD-1 enhanced cancer proliferation and inhibited cell apoptosis *in vitro* and *in vivo*. Mechanistically, PD-1 binds to the downstream MOB1, thereby inhibiting its phosphorylation. Moreover, greater synergistic tumor suppression *in vitro* resulted from combining Hippo inhibitors with *anti*-PD-1 treatment compared with the suppression achieved by either single agent alone. Additionally, Hippo downstream targets, CYR61 (CCN1) and CTGF (CCN2), were directly affected by PD-1 mediated Hippo signaling activation in concert with survival outcomes. Finally, the formulated nomogram showed superior predictive accuracy for OS in comparison with the TNM stage alone. Therefore, PD-1 immunotherapy in combination with Hippo pathway inhibitors may optimize the anti-tumor efficacy in PDAC patients via targeting cell-intrinsic PD-1.

1. Introduction

Pancreatic ductal adenocarcinoma (PDAC) is one of the most fatal and refractory malignant cancers with a low 5-year survival of less than 8% [1,2]. For PDAC patients, surgery is considered to be the only curative treatment in concert with chemotherapy and/or radiotherapy [3]. Although the validity of immunotherapy has been evaluated in several solid tumors [4,5], its efficacy remains poor in PDAC probably due to the protective stromal barriers and inhibitory immune microenvironment [6–8].

Immune checkpoint inhibitors (ICIs) are newer, immunotherapy-based drugs that have been verified to improve survival in several malignant cancers, including melanoma, renal cancer, and nonsmall cell lung cancer (NSCLC) [9–11]. Programmed cell death protein-1 (PD-1) is commonly known as one of the inhibitory immune checkpoints on activated T cells, NK cells, and B cells, which interacts with the programmed death ligand 1 (PD-L1) on cancer cells to create second inhibitory signaling [12–14]. PD-1/PD-L1 mutual interaction suppresses the cytotoxic T cell activity and drives T cell dysfunction [15,16]. Intriguingly, PD-1 expression has been reported to be detected on melanoma [17], hepatocellular carcinoma [18], and NSCLC [19] cells. Kleffel et al. [17] and Li et al. [18] demonstrated that cancer cell-intrinsic PD-1 promoted cancer proliferation and growth in melanoma and hepatocellular carcinoma, respectively; however, intrinsic PD-1 presented as a protective factor in NSCLC [19]. Nevertheless, the expression of cell-intrinsic PD-1 in PDAC is still not well understood.

** Corresponding author. Department of General Surgery, Zhongshan Hospital, Fudan University, 180 Fenglin Road, Shanghai, 200032, China.
* Corresponding author. Department of Surgery, The Sol Goldman Pancreatic Cancer Research Center, The Johns Hopkins University School of Medicine, 600 N. Wolfe Street, Baltimore, MD, 21287, USA.
E-mail addresses: jyu41@jhmi.edu (J. Yu), lou.wenhui@zs-hospital.sh.cn (W. Lou).
[1] NP, SSG, and HLY contributed equally to this work.

https://doi.org/10.1016/j.canlet.2019.06.013
Received 28 March 2019; Received in revised form 17 June 2019; Accepted 19 June 2019
0304-3835/ Published by Elsevier B.V.

Since Yao et al. [20] reviewed that tumor intrinsic PD-1 mRNA expression was correctly detected in PDAC from the Cancer Genomic Atlas (TCGA) project and that it showed significantly different expression in pancreatic cancer cell lines from the Cancer Cell Line Encyclopedia (CCLE), cell-intrinsic PD-1 may be similarly expressed in PDAC. However, the function and mechanism of cell-intrinsic PD-1 regulation remain unclear.

Here, we report that cell-intrinsic PD-1 is positively expressed in PDAC cell lines and higher content is correlated with poorer overall survival (OS) in PDAC patients undergoing radical resection. PD-1 overexpression (PD-1 OE) in pancreatic cancer cells promotes tumor growth and suppresses cell apoptosis required for PD-L1 independently of the immunological environment. In contrast, PD-1 knockdown (PD-1 KD) or blockade eliminates this impact. A potential mechanism is that cell-intrinsic PD-1 interacts with Mps1-One binder (MOB1) to inhibit its phosphorylation, and then promotes the Hippo signal pathway to activate its downstream targets, cysteine-rich angiogenic inducer 61 (CYR6, CCN1) and connective tissue growth factor (CTGF, CCN2). More importantly, Hippo pathway inhibitors, together with *anti*-PD-1 immunotherapy, show superior synergistic tumor inhibition, and the formulated nomogram containing CYR61, CTGF, and AJCC 8th staging provides a robust prognostic model for resected PDAC patients.

2. Materials and methods

2.1. Clinical specimens and follow-up

The clinical samples for tissue microarray (TMA) were taken from 90 resected PDAC patients in Zhongshan Hospital, Fudan University from September 2012 to May 2016, coupled with detailed information as previously described [13]. Following surgery, all patients were monitored until December 2016 in the Department of General Surgery, Zhongshan Hospital, Fudan University, Shanghai, China. The use of tumor specimens was approved by the Ethics and Research Committees of Zhongshan Hospital, Fudan University. The OS was calculated as the time interval between surgery and death or December 2016.

2.2. Ethics approval and consent to participate

The Clinical Research Ethics Committee of Zhongshan Hospital approved the ethical use of human subjects for this study.

2.3. Pancreatic cancer cell lines

Human pancreatic cancer cell lines, PANC-1, MIA-PaCa-2, BxPC-3 and Sw1990, were received from the Chinese Academy of Sciences, Shanghai, China. PANC-1 and MIA-PaCa-2 were cultured in high-glucose Dulbecco's Modified Eagle's Medium (DMEM) (Gibco, Carlsbad, CA, USA) supplemented with 10% fetal bovine serum (Gibco), 100 U/mL penicillin and 100 U/mL streptomycin (Gibco) in a humidified 37 ˚C and 5% CO2 incubator, while BxPC-3 and Sw1990 were cultured in RPMI-1640 medium (Gibco) instead of DMEM. In addition, 2.5% horse serum was added to the MIA-PaCa-2 cultures.

2.4. Cell transfection

Two lentiviral vectors were constructed containing Ubi-PD-1-3FLAG-SV40-EGFP-IRES-puromycin and hU6-PD-1-ubiquitin-EGFP-IRES-puromycin (GeneChem, Shanghai, China). The primer sequences for human PD-1 gene fragments were 5′-GAGGATCCCCGGGTACCGGTCGCCACCATGCAGATCCCACAGGCGCCCTG-3’ (forward) and 5′-TCCTTGTAGTCCATACCGAGGGGCCAAGAGCAGTGTCCATC-3’ (reverse). The human PD-1 shRNA target logical sequence was 5′-CTAGAGAAGTTTCAGGGAA-3’. The Ubi-3FLAG-SV40-EGFP-IRES-puromycin and hU6-control-ubiquitin-EGFP-IRES-puromycin lentiviral vectors were used as controls. Stably transfected clones for PD-1 were validated by quantitative real-time polymerase chain reaction (qRT-PCR) and western immunoblot analysis.

2.5. RNA isolation, reverse transcription and qRT-PCR

Total RNA was isolated from the human pancreatic cancer cell lines (PANC-1, MIA-PaCa-2, BxPC-3 and Sw1990). PrimeScript® reverse transcriptase Master Mix (Takara Bio Inc., Otsu, Shiga, Japan) was used for the cDNA synthesis reactions, and SYBR Premix Ex Taq (Takara Bio Inc.) was used to amplify the reverse transcribed products for qRT-PCR analysis according to the manufacturer's instructions. The primers used for qRT-PCR were: human PDCD1, 5-CCAGGATGGTTCTTAGACTCCC-3 (forward) and 5- TTTAGCACGAAGCTCTCCGAT-3 (reverse); Human GAPDH, 5- GGAGCGAGATCCCTCCAAAAT-3 (forward) and 5-GGCTG TTGTCATACTTCTCATGG-3 (reverse). PCRs were run in triplicate in 20 μL reactions under conditions of 95 ˚C for 30 s, 40 cycles of 95 ˚C for 5 s, 60 ˚C for 34 s and melting curve of 95 ˚C for 10 s, 60 ˚C for 60 s, 95 ˚C for 15 s using the ABI 7500 Real-Time PCR (Applied Biosystems, Foster City, CA, USA). The relative mRNA expression of transcripts was normalized to GAPDH and analyzed by using the $2^{(-\triangle\triangle Ct)}$ method.

2.6. Proliferation assay

Two thousand cells suspended in 100 μL medium were seeded in each well of 96-well plates, and cell viability and proliferation ability were measured at 12, 24, 48, and 72 h. The cell counting kit-8 (CCK-8) reagent (Dojindo Molecular Technologies, Gaithersburg, MD, USA) was added into the culture medium resulting in a 10% CCK-8 working solution and incubated for an additional 2 h. A microplate reader (Bio-Rad, Hercules, CA, USA) was used to measure the cell viability and proliferation ability in each well according to the absorbance at a wavelength of 450 nm. In addition, 300 MIA-PaCa-2 cells and 500 BxPC-3 cells were seeded in each well of six-well plates for colony formation assays and cultured at 37 ˚C with 5% CO_2 in an incubator for two weeks. After the incubation, cells were washed with phosphate buffered saline (PBS), fixed with 1% paraformaldehyde for 30 min, and stained with 0.1% crystal violet (Beyotime, Shanghai, China) for an additional 30 min. Image-Pro Plus 5.0 software (Media Cybernetics, Bethesda, MD, USA) was used to count the numbers of cell colonies. Then, PD-1-OE cells treated with suitable drugs for 48 h were analyzed for drug treatment proliferation. Yes-associated protein-transcriptional enhanced associate domain (YAP-TEAD) Inhibitor 1 (Peptide 17, Selleck, Houston, TX, USA) was administered at a concentration of 200 nM, while 50 μg/ml of anti-human PD-1, PD-L1, and relevant isotype control mAb (BioXcell, West Lebanon, New Hampshire, USA) were used in *vitro*.

2.7. Flow cytometry (FCM)

PD-1-APC antibody (Biolegend, San Diego, California, USA) and PD-L1-PE antibody (BD Biosciences, Franklin Lakes, NJ, USA) were used to examine the PD-1 and PD-L1 expression on the surface of wild-type or transfected pancreatic cancer cell lines. The mean fluorescence intensity (MFI) of staining for each marker was analyzed. After a 48 h treatment, cell lines were analyzed for apoptosis by staining with annexin V-APC and PI (BD Bioscience). The target populations were identified by FACS Aria II flow cytometer (BD Bioscience).

2.8. Western blotting analysis

Total proteins were extracted from pancreatic cancer cell lines with RIPA (1%PMSF) and protease inhibitors and were quantified by the BCA Protein Assay Kit (Beyotime). The proteins were separated by 10% sodium dodecyl sulfate-polyacrylamide gel electrophoresis (SDS–PAGE, Beyotime) and then electrotransferred onto polyvinylidene difluoride (PVDF) membranes (Millipore, Billerica, MA, USA). A 5% nonfat milk

in TBS-T solution was used to block the PVDF membranes, and then primary antibodies with 1:1000 dilutions were incubated overnight. The next day, the PVDF membranes were incubated with the HRP-conjugated second antibody (Beyotime) at 1:5000 dilutions at room temperature. Then, the expression of the relevant protein was detected with Tanon 5200 Image System (Tanon, Shanghai, China). In this study, *anti*-GAPDH (Cell Signaling Technology, Danvers, MA, USA), *anti*-PD-1 (R&D Systems, Tustin, California, USA and Abcam, Cambridge, UK), *anti*-PD-L1 (Cell Signaling Technology), anti-MOB1 (Cell Signaling Technology), *anti*-phospho-MOB1 (pMOB1, Cell Signaling Technology), *anti*-LATS1 (Cell Signaling Technology), *anti*-phospho-LATS1 (pLATS1, Cell Signaling Technology), anti-YAP (Cell Signaling Technology), *anti*-phospho-YAP (pYAP, Cell Signaling Technology), *anti*-CTGF (Cell Signaling Technology) and *anti*-CYR61 (Cell Signaling Technology) monoclonal antibodies (mAbs) were used. PD-1-OE cells were previously treated with 50 μg/ml of anti-human PD-1, PD-L1 or isotype control mAb (BioXcell) and with YAP-TEAD Inhibitor1 (Peptide 17) at different concentration for 48 h and then used for Western blot analysis.

2.9. Immunohistochemistry (IHC) and immunofluorescence (IF)

HE staining was administered for formalin-fixed, paraffin-embedded (FFPE) xenografted tumor specimens and FFPE tissue TMA specimens. *Anti*-PD-1(Abcam), anti-CD8 (Cell Signaling Technology), anti-MOB1 (Cell Signaling Technology), *anti*-Ki-67 (Abcam), *anti*-CTGF (Cell Signaling Technology) and *anti*-CYR61 (Cell Signaling Technology) monoclonal antibodies were applied for IHC staining as previously described [13].

The expression of PD-1, CYR61, and CTGF in TMA specimens was independently calculated by two authors blinded to section treatment. The immunoreactivity scores of PD-1, CYR61, and CTGF in the TMA specimens were derived by multiplying the percentage of immunoreactive cells and the intensity of IHC staining, which ranged from 0 to 12. As a result, specimens with a final staining score of ≥ 6 were labeled as high expression, while those of < 6 were classified as low expression.

IF staining was performed on the cultured pancreatic cancer cells. Anti-MOB1 (Cell Signaling Technology) was used as the primary antibody for 1 h at room temperature. Then, coverslips were incubated with the second antibody with red fluorescence detection for 1 h, and PD-1 expression was detected with the green fluorescence by intrinsic GFP.

2.10. Immunoprecipitation and proteome analysis

Proteins were extracted from cell lysates with lysis buffer. Protein A/G beads (Thermo Fisher Scientific, Waltham, MA, USA) and antibodies were added to protein lysates, then incubated overnight. Proteins from the beads were subjected to Western blot, in-gel cut and digestion, and then proteome analysis by liquid chromatography–mass spectrometry/mass spectrometry (LC-MS/MS) performed by Bangfei Biotechnology Co. (Beijing, China).

A Q Exactive mass spectrometer, which was coupled to Easy nLC (Thermo Fisher Scientific), was used to perform the experiments. A C18-reversed-phase column packed with RP-C18 5 μm resin in 0.1% formic acid in high performance liquid chromatography (HPLC)-grade water bound the peptide mixture and then separated it with a linear gradient of 0.1% formic acid in 84% acetonitrile at a flow rate of 250 nl/min controlled by IntelliFlow technology over 60 min. Moreover, by a data-dependent top 10 method choosing the most abundant precursor ions from the survey scan (300–1800 m/z) for high-energy collisional dissociation (HCD) fragmentation dynamically, MS data was acquired, and the target value determination relied on predictive Automatic Gain Control (pAGC). It was observed that the underfill ratio specified the target value with the minimum percentage likely to be reached at the maximum fill time, which was defined as 0.1%, and the normalized collision energy was 27 eV. Peptide recognition mode was enabled to run in the instrument.

MASCOT engine (Matrix Science, London, UK) against uniprot_Human_173837_201807027 was used for MS/MS spectra analysis. The options of peptide mass tolerance = 20 ppm, enzyme = Trypsin, MS/MS tolerance = 0.1 Da, missed cleavage = 2, variable modification:oxidation(M), fixed modification: carbamidomethyl (C), ion score > 20 and FDR < 0.01 at the peptide and protein levels were applied for protein identification.

2.11. Mouse xenograft study

Forty-eight male, 4-5-week-old NOD/SCID mice (Shanghai SLAC Laboratory Animals Co., Ltd, Shanghai, China) were raised in a specific pathogen free (SPF) environment. The China Animal Welfare Guidelines were followed during the experimental animal procedures all the time. The Institutional Animal Care and Use Committee in Zhongshan Hospital, Fudan University, approved this study protocol. The NOD/SCID mice were randomly assigned to two cohorts, and in each group, stable PD-1-OE, PD-1-KD or vector control cells were subcutaneously inoculated into the right subscapular region with 1×10^7 cells/inoculum. Tumor volume was calculated by (length × width^2)/2, and the tumor length and width were measured weekly.

2.12. Statistical analyses

SPSS 21.0 software (IBM Corporation, Armonk, NY, USA) and R project version 3.4.4 (R Foundation for Statistical Computing, Vienna, Austria) were used for statistical analysis. The correlations between PD-1, CYR61, and CTGF expression and clinicopathological characteristics were analyzed by Pearson Chi-squared test, Fisher's exact test or Mann–Whitney *U* test, as appropriate. Kaplan-Meier survival curves and a log-rank test were used to estimate median OS and compare survival outcomes. Univariate and multivariate analyses of demographic and clinicopathologic variables were performed using a Cox proportional hazards model. The categoric values of experiments were presented as the mean ± standard deviation $\bar{x}\pm s$.The quantitative data of two groups were compared by two-tailed Student's t-tests, while data with multigroup comparisons were assessed using one-way ANOVA, and then, the LSD or Tamhane method was applied for further studies. A value of $p < 0.05$ was considered statistically significant. Kaplan–Meier survival curves, nomogram, calibration curves, and decision curve analysis (DCA) were depicted with an R project as previously described [2]. The Western blot bands were analyzed with ImageJ software (National Institutes of Health, Bethesda, MD, USA). Tumor growth curves were plotted by GraphPad Prism 6.0 (GraphPad Software, La Jolla, CA, USA).

3. Results

3.1. Cell-intrinsic PD-1 in PDAC correlated with poor prognosis

The results of IHC staining of TMA specimens are shown in Fig. 1A and in Table S1. PD-1 expression was mainly located on the cytoplasm and surface of the tumor cells at low (40 ×) and high (400 ×) magnification, and there was no expression in tumor-adjuvant pancreatic tissues. Through analysis, PD-1 was highly expressed in 27.8% (25/90) of PDAC specimens. The relationships between PD-1 staining and other clinicopathological characteristics are shown in Table S2, and the results showed no significant correlation with routine blood and pathological indicators (all $p > 0.05$).

The survival details of a total of 90 PDAC patients undergoing pancreatectomy were previously described [13]. Cell-intrinsic PD-1 was significantly considered as a prognostic characteristic associated with OS in the Kaplan–Meier curves analysis, and patients with higher PD-1 expression tended to have a shorter survival time (12.0 vs. 19.0

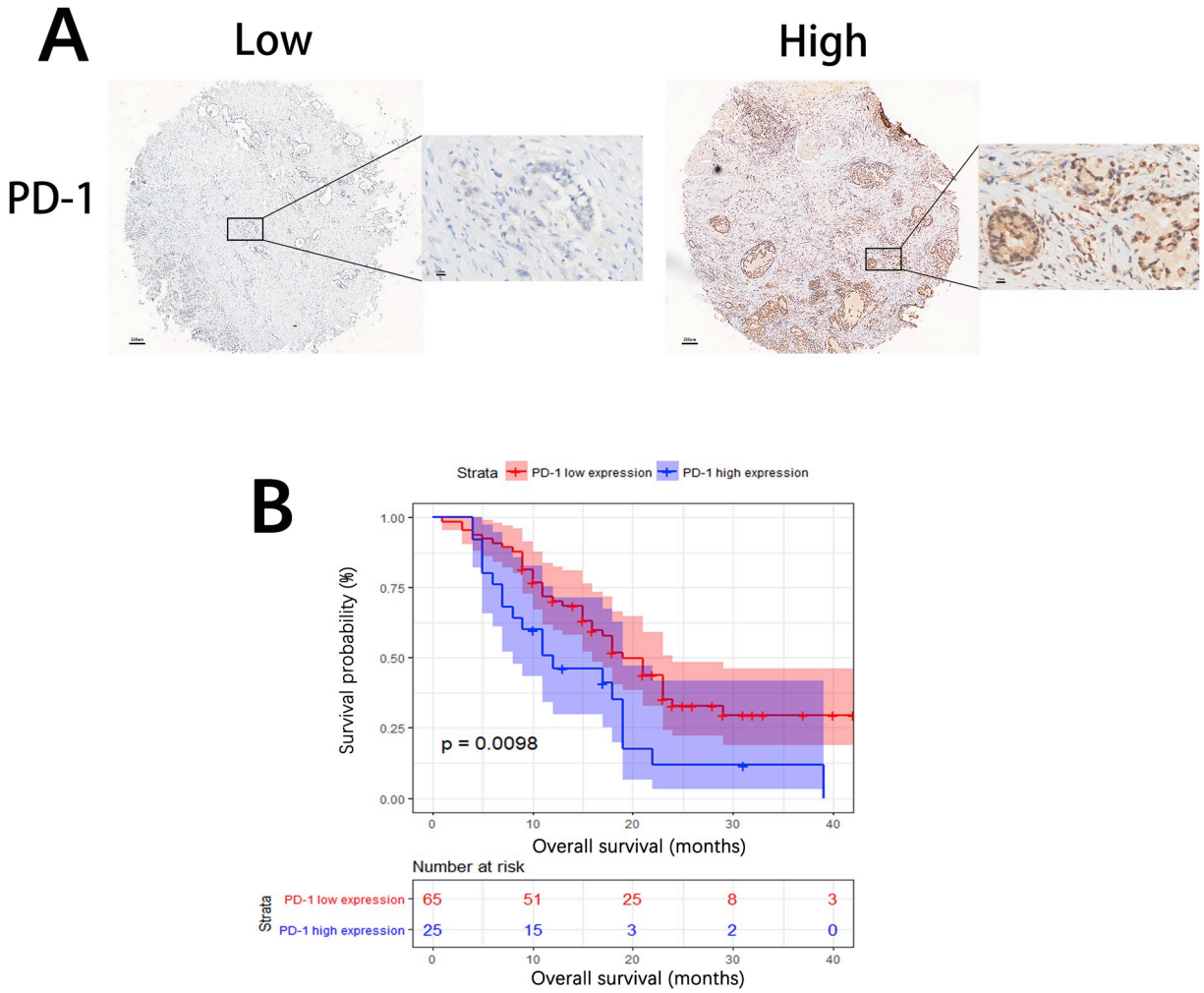

Fig. 1. The immunohistochemistry staining for PD-1 in PDAC tissue microarray and its associated survival. (A) The representative images illustrating low and high expression of PD-1 (× 40 low-power and × 400 high-power fields respectively). (B) Kaplan–Meier survival curves of PD-1 analyzed by Log-rank test.

months) (Fig. 1B, $p = 0.010$). Concomitantly, significant risk characteristics under univariate analysis were subjected to Cox proportional hazards multivariate analysis (Table S3). The results of multivariate analysis revealed that N classification ($p = 0.043$, hazard ratio [HR] = 2.360, 95% confidence interval [CI] = 1.028–5.418) and PD-1 expression ($p = 0.014$, HR = 2.017, 95% CI = 1.155–3.523) remained independently and negatively associated with OS. The 1-year and 3-year OS rate of PDAC patients with higher PD-1 expression was 46.2% and 11.7%, respectively, while those of PDAC patients with lower PD-1 expression was 70.2% and 29.5%, respectively.

3.2. Cell-intrinsic PD-1 in PDAC promoted cancer proliferation

As we hypothesized that cell-intrinsic PD-1 was expressed in pancreatic cancer cells, we examined its expression in four pancreatic cancer cell lines. The qRT-PCR and Western blot results showed intrinsic PD-1 was correctly represented in pancreatic cancer cells (Fig. 2A and B). In addition, four pancreatic cancer cell lines staining with PD-1-APC mAb compared to IgG-APC mAb showed that expression of PD-1 located on the surface was higher in MIA-PaCa-2 cells than in BxPC-3 or PANC-1 cells, and Sw1990 cells had the lowest expression (Fig. 2C).

Then, compared with controls, stable PD-1 overexpressing (PD-1-OE) and PD-1 knockdown (PD-1-KD or PD-1-shRNA) MIA-PaCa-2 and BxPC-3 cell lines, which had significantly increased or blocked PD-1 protein expression, respectively, were generated (Fig. 2D and E). Concurrently, the exogenous PD-1 overexpression was also precisely located on the surface of PD-1-OE MIA-PaCa-2 and BxPC-3 cells (Fig. 2F and G). To determine the functional phenotype of cell-intrinsic PD-1, we used the MIA-PaCa-2 PD-1 OE and vector control cells for the RNA sequencing. Ingenuity pathway analysis (IPA) showed that cell-intrinsic PD-1 was mainly associated with cell death and cancer survival (Figs. S1A–C).

Cell proliferation and clone formation ability were primarily assessed with the CCK-8 proliferation and clone formation assays, which showed that the degree of proliferation and clone formation was highly increased in PD-1-OE MIA-PaCa-2 (Fig. 3A–C) and BxPC-3 cells (Figs. S2A–C) compared to vector controls. In contrast, PD-1-KD BxPC-3 cells (Fig. 3D–F) and MIA-PaCa-2 cells (Figs. S2D–F) showed the opposite trends in proliferative responses. In PD-1-OE MIA-PaCa-2 cells, the cell apoptosis rate by FCM was 8.26 ± 1.06% compared with that of 13.77 ± 0.86% in vector control cells (Fig. 3G and H), while the cell apoptosis rate of PD-1-KD BxPC-3 cells was 20.12 ± 1.14% compared with that of 12.74 ± 0.55% in shRNA control cells (Fig. 3G and I). The synergistic effects were also tested in PD-1-KD MIA-PaCa-2 and PD-1-OE BxPC-3 cells (Fig. S2G).

To further reveal the *in-vivo* proliferative effect of cell-intrinsic PD-1 on PDAC growth, immunocompromised (T- and B cell-deficient) NOD/SCID mice were injected with MIA-PaCa-2 and BxPC-3 cells transfected with the relevant lentiviral vectors, and then tumor growth was measured for proliferation ability. As the results showed, the xenograft tumor sizes in the PD-1 OE cohort were significantly larger than those

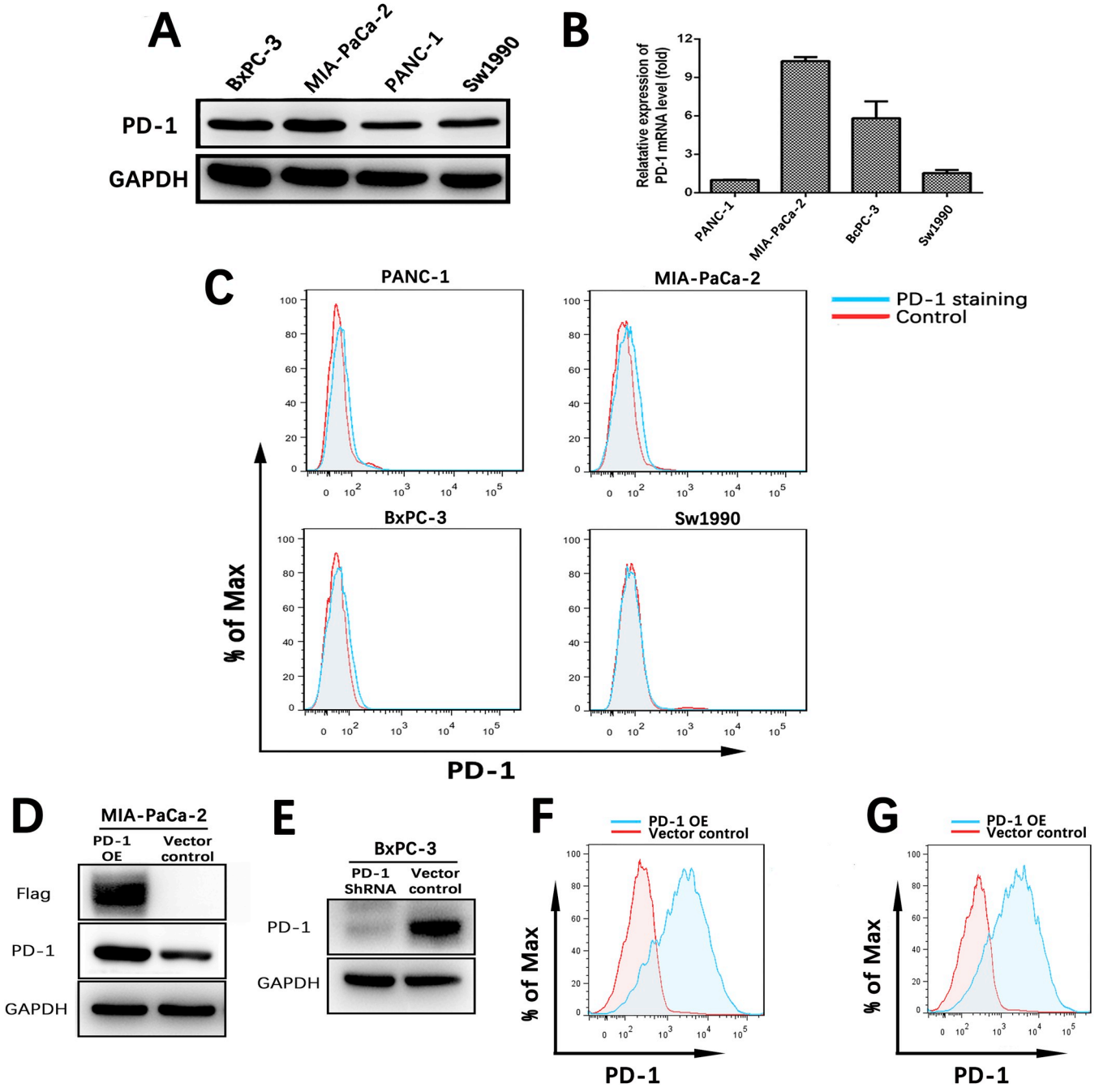

Fig. 2. Expression of PD-1 in wide-type and transfected PDAC cells. (A) Western blot analysis and (B) qRT-PCR analysis for PD-1 in four wild-type PDAC cells. (C) The mean fluorescence intensity (MFI) of PD-1 expression on the surface of four wild-type PDAC cells compared with cells with IgG staining. Western blot analysis of PD-1 in (D) MIA-PaCa-2 transfected with PD-1 overexpressed plasmid and vector control and (E) BxPC-3 transfected with PD-1 shRNA plasmid and vector control. The MFI of PD-1 expression on the surface of PD-1 overexpressing (F) MIA-PaCa-2 and (G) BxPC-3 compared with its relative vector control.

in the vector control cohort ($p < 0.01$; Fig. 3J and S2H), and the xenografts of the PD-1 shRNA cohort were significantly smaller than the vector controls ($p < 0.05$; Fig. 3K and S2I). Furthermore, Ki-67, as a proliferation marker, was analyzed in the FFPE specimens of xenografts, which showed that, compared with the vector controls, the proliferation rate was significantly enhanced in the PD-1 OE cohort xenografts, while the proliferation rate in the PD-1 shRNA cohort xenografts was dramatically decreased (Fig. 4E and Fig. S3C). Hence, PD-1 OE cells promoted, and PD-1 KD cells suppressed, pancreatic cancer growth in NOD/SCID mice when compared with their controls, which implicates PD-1 in tumorigenesis and progression.

3.3. Cell-intrinsic PD-1 activated the hippo signaling pathway, which requires PD-L1

Through the signal pathway analysis of the RNA sequencing data, we observed that the highest activation pathway was the YAP-mediated signaling pathway (Fig. S1E). To investigate the molecular mechanism of cell-intrinsic PD-1 contributing to PDAC growth, immunoprecipitation and LC-MS/MS analyses of stable PD-1 OE cells or vector controls were performed to identify different components in the complexes of proteins. PD-1-associated protein complexes were isolated from PD-1 OE and vector control MIA-PaCa-2 cells via using anti-Flag mAb-coated paramagnetic beads. The beads coated with anti-Flag mAbs bound PD-1

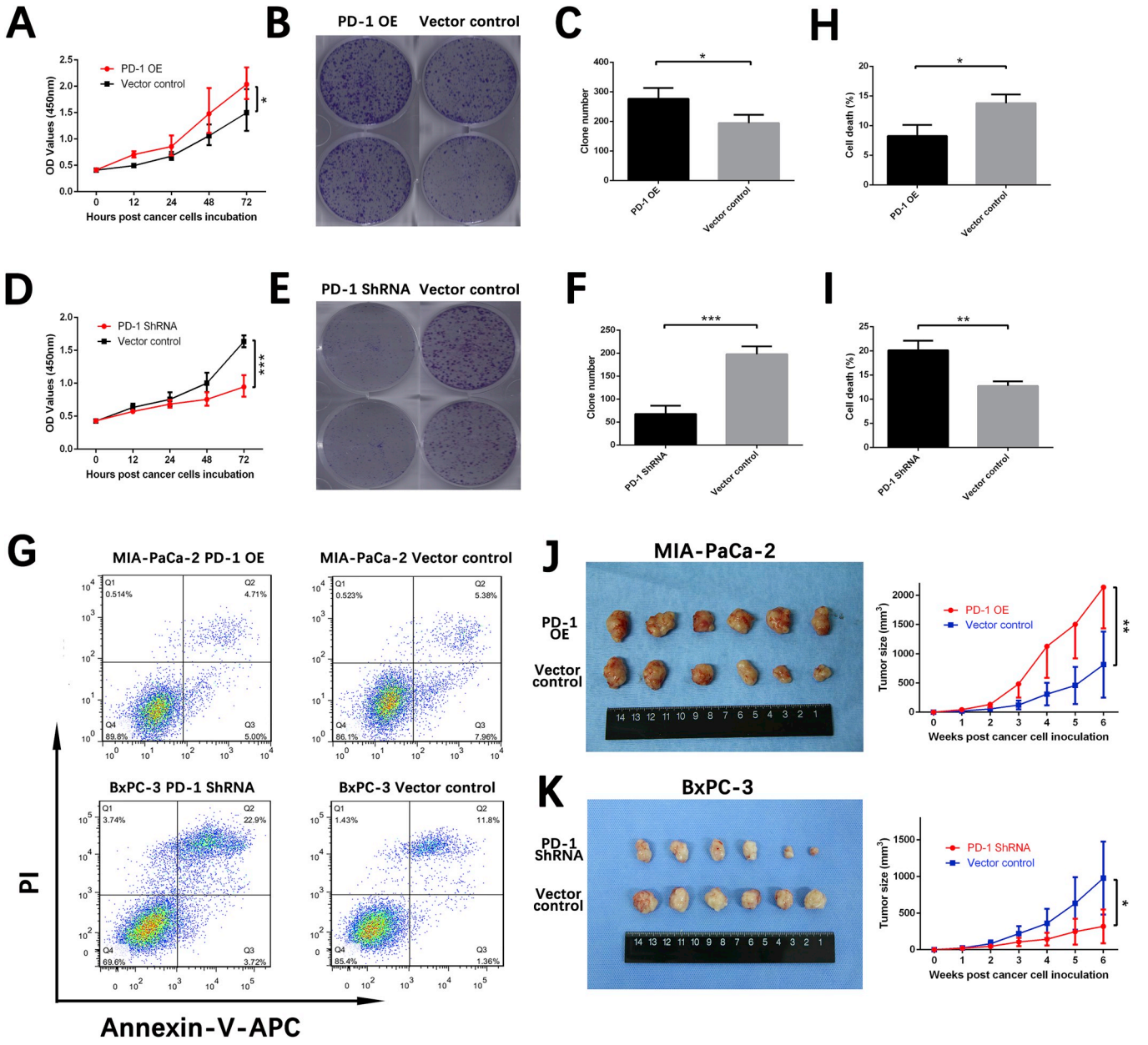

Fig. 3. Cell-intrinsic PD-1 in PDAC promotes cell proliferation and tumor growth. (A) CCK-8 assay at 0, 12, 24, 48, 72 h and (B, C) clone formation assay for 2 weeks for cell proliferation after PD-1 overexpression in MIA-PaCa-2 cells. (D) CCK-8 assay at 0, 12, 24, 48, 72 h and (E, F) clone formation assay for 2 weeks for cell proliferation after PD-1 shRNA transfection in BxPC-3 cells. (G, H, I) Flow cytometry data showing cell apoptosis by the vector controls and PD-1 overexpression in MIA-PaCa-2 cells and PD-1 knockdown in BxPC-3 cells. Tumor sizes and growth rates (means ± SD) of the (J) PD-1 overexpression versus vector control MIA-PaCa-2 cells and the (K) PD-1 knockdown versus vector control BxPC-3 cells in NOD/SCID mice models. *, p-value < 0.05; **, p-value < 0.01; ***, p-value < 0.001.

and its associated proteins, and then the protein complexes were separated, purified and analyzed by MS.

One hundred seventy proteins were identified by proteomic analysis within at least 99% confidence. There were 47 overlapped proteins (27.6%) identified between the complexes from PD-1 OE cells and vector controls. Meanwhile, 78 proteins (45.9%) were unique to the compounds related to PD-1 that were detected in the complexes from PD-1 OE cells (Fig. S1D). In these novel proteins in PD-1 OE cells, we found the MOB1 protein as expected, which was thought to be a medium protein towards the Hippo pathway. For these reasons, we speculated that cell-intrinsic PD-1 might promote tumor growth by associating with MOB1 and then activating Hippo signaling pathways.

To test our hypothesis, repeated immunoprecipitation and immunofluorescence staining were performed to validate the results. As the immunoprecipitation results showed, endogenous MOB1 was co-immunoprecipitated by anti-Flag mAbs, whereas the endogenous PD-1 and Flag-tagged PD-1 were co-immunoprecipitated by anti-MOB1 mAbs reciprocally in PD-1 OE MIA-PaCa-2 cells (Fig. 4A). Confocal microscopy revealed that PD-1 was localized to the cell membrane and cytoplasm, which was associated with the expression of MOB1 (Fig. 4B). In addition, we further assessed the effect of cell-intrinsic PD-1 expression on Hippo signaling by examining MOB1, Large Tumor Suppressor homolog kinases 1 (LATS1), YAP, and their phosphorylation. The results showed that the Hippo signal pathway was notably enhanced in MIA-PaCa-2 and BxPC-3 cells with PD-1 transfection (Fig. 4C and S3A), while it significantly declined in PD-1 KD cells (Fig. 4D and S3B). In addition, IHC staining of tumor specimens demonstrated that MOB1 was markedly enhanced in MIA-PaCa-2 and BxPC-3 cells with PD-1 transfection, whereas MOB1 in PD-1 KD cells was dramatically suppressed (Fig. 4E and S3C). These data revealed that PD-1 interacted

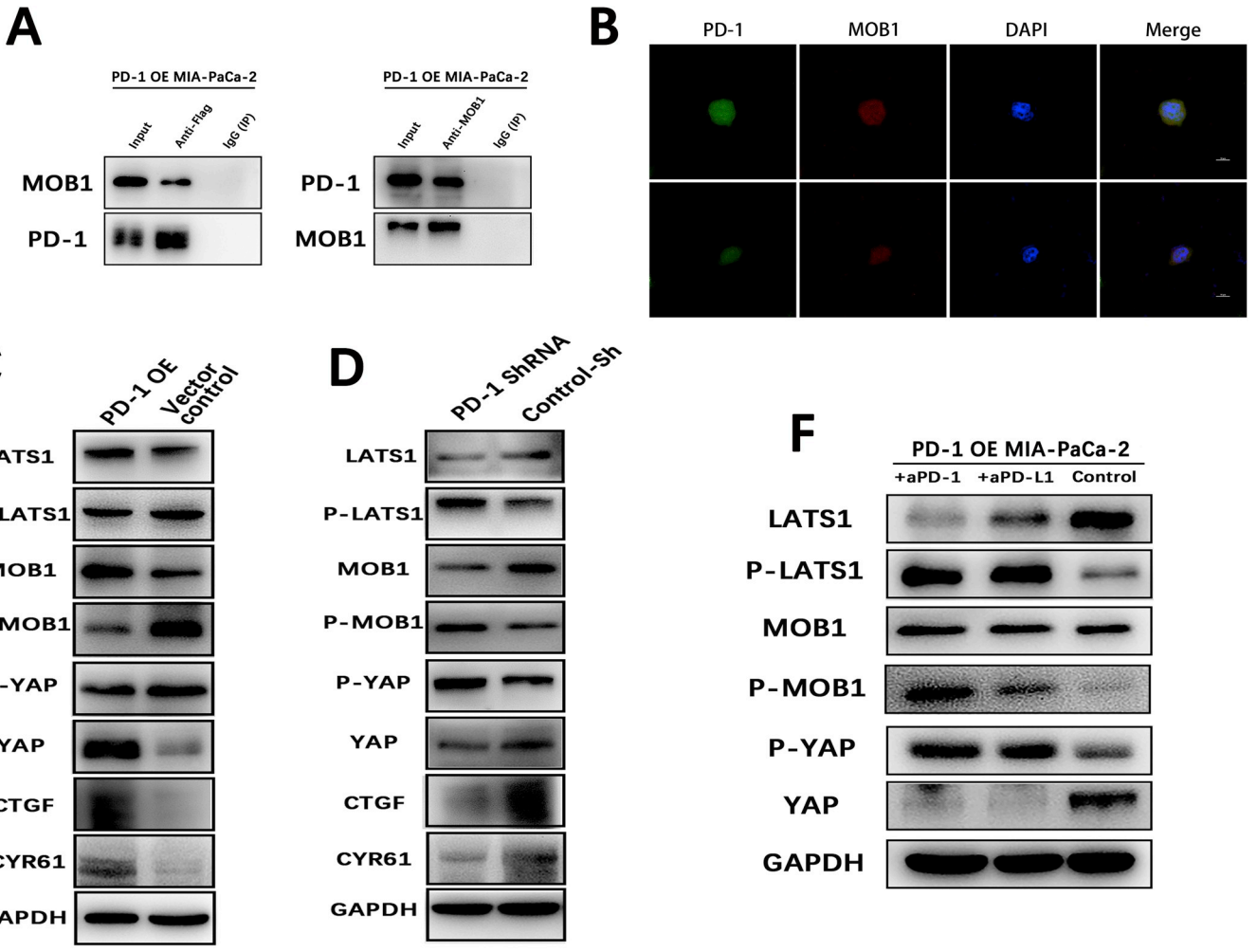

(caption on next page)

Fig. 4. Cell-intrinsic PD-1 activates the Hippo signaling pathway associating with MOB1, which requires PD-L1. (A) Co-immunoprecipitation assays in MIA-PaCa-2 transfected with a vector containing flag-tagged PD-1 and IgG used as control. (B) Confocal microscopy scan of immunofluorescence staining assays showing PD-1 (green) association with the expression of MOB1 (red) in the PD-1 overexpression (OE) MIA-PaCa-2 cells. Western blot analysis of Hippo signaling pathway changes when (C) PD-1 OE in MIA-PaCa-2 cells and (D) PD-1 knockdown in BxPC-3 cells. (F) Western blot analysis of Hippo signaling pathway changes in the PD-1 OE MIA-PaCa-2 cells treated with 50 μg/ml of anti-human PD-1 and PD-L1 antibodies compared with blank control. (E) Representative HE and immunohistochemistry staining of xenograft tumors from NOD/SCID mice subcutaneously injected with transfected MIA-PaCa-2 cells for the expressions of PD-1, Ki-67, and MOB1. (For interpretation of the references to colour in this figure legend, the reader is referred to the Web version of this article.)

to MOB1 and physically modulated its phosphorylation.

To further examine the effect of cell-intrinsic PD-1 required for PD-L1, we first tested the PD-L1 expression in cancer cells. The WB results showed that both MIA-PaCa-2 and BxPC-3 wild-type and PD-1-OE cells exhibited PD-L1 expression, and the FCM results further showed that both cell lines had high PD-L1 expression on their surface (Figs. S3D and S3E). Then, we treated the PD-1-OE cells with *anti*-PD-L1 antibodies, and the results showed the activated Hippo pathway by PD-1 regulator was reversibly suppressed by PD-L1 blockade (Fig. 4F and S3F).

3.4. PD-1 blockade in combination with a hippo signaling inhibitor in vitro suppressed PDAC growth

To verify the inhibitive effect of cell-intrinsic PD-1 in proliferation, we used *anti*-PD-1 antibody and YAP-TEAD Inhibitor 1 (Peptide 17) in an attempt to suppress the Hippo pathway. First, we validated the efficacy of Peptide 17 in the inhibition of the Hippo pathway, which showed an excellent performance in reversing the effect of PD-1 OE (Fig. 5A). Next, we treated the MIA-PaCa-2 and BxPC-3 PD-1 OE cells with *anti*-PD-1 antibody and Peptide 17, and then the WB results showed that PD-1 blockade effectively inhibited the Hippo pathway activation (Fig. 4F and S3E). In the *in vitro* functional analysis with interventions, the CCK-8 and clone formation results revealed that PD-1 blockade in combination with Peptide 17 led to a more significant decrease in proliferation than control or single treatment (Fig. 5B and C). Apoptosis analysis also revealed a higher apoptosis rate in cells receiving the combination treatment (Fig. 5D). It is important to note that *anti*-PD-1 therapy may reduce the cancer cell population, and higher cell death may be achieved with *anti*-PD-1 in concert with Peptide 17 treatments.

3.5. Nomogram containing CYR61/CTGF and AJCC 8th system showed an excellent predictive role

CYR61 and CTGF are tumorigenesis genes operating downstream of the Hippo pathway [21–24]. As the results showed, MIA-PaCa-2 and BxPC-3 cells transfected with PD-1 vector showed significantly increased CYR61 and CTGF expression (Fig. 4C and S3A). In further treatment with Peptide 17, CYR61 and CTGF showed decreased expression in PD-1 OE cells (Fig. 5A). Thus, CYR61 and CTGF may be the dominating targets that are regulating cell proliferation and death.

We further analyzed the CYR61 and CTGF expression in the TMA of PDAC. The IHC results showed that both CYR61 and CTGF were located in the cytoplasm and associated with OS. Higher expression of CYR61 or CTGF, was associated with higher patient OS (both $p < 0.001$, Fig. 6A–C). Further analysis was conducted to determine that CYR61 expression was significantly correlated to gender ($p = 0.014$) and CA19-9 ($p = 0.020$), while CTGF expression showed a strong association with T classification ($p = 0.007$) and PD-1expression ($p = 0.048$) (Table S4). The results showed that the male patients or patients with higher CA19-9 might exhibit higher CYR61 expression, and higher T classification or higher PD-1 expression seemed to cause higher CTGF expression. When CYR61 and CTGF were subjected to multivariate analysis, both CYR61 and CTGF were found to be independent risk factors for OS (Table S5).

To obtain a more precise predictive model, we tried to formulate a nomogram containing AJCC 8th TNM staging, CYR61, and CTGF expression. The C-index of the formulated nomogram for OS prediction was 0.720 ($p < 0.001$, 95% CI, 0.712–0.728), while the C-index for the TNM staging system alone was only 0.585 ($p < 0.05$, 95% CI, 0.577–0.593). In addition, the actual observation and nomogram prediction of 1-, 2- and 3-years OS following surgery were depicted by calibration curves, which exhibited optimal consistency (Fig. 6E). Then, a novel evaluation method, DCA [25], was administered to highlight predictive models with clinical net benefits, which showed that the formulated nomogram had a wider range of threshold probability with superior net benefits and improved performance for predicting OS at 1 and 2 years when compared with the AJCC 8th TNM staging system (Fig. 6F).

4. Discussion

In this study, we obtained new information about the functions of the cell-intrinsic PD-1 pathway in PDAC. From an entirely novel viewpoint, PD-1 is no longer expressed predominantly on immunogenic cells [26]. We found that pancreatic cancer cell lines and PDAC tissue specimens also expressed PD-1, and this expression was confirmed to correlate with survival. PD-L1 expressed on PDAC was previously reported as a significant indicator for survival outcomes [27,28] and multiple therapies targeting to PD-L1 revealed an unexpected result [29,30]. However, we evaluated the prognostic role of cell-intrinsic PD-1 by using TMA from resected PDAC patients. Patients with high cell-intrinsic PD-1 expression had an unsatisfactory OS. In contrast, PDAC patients with low PD-1 expression had a more favorable prognosis (19.0 months vs. 12.0 months, respectively). Moreover, cell-intrinsic PD-1, as well as N classification, was further confirmed as an independent prognostic factor through multivariate analysis.

So far, the role of PD-1 has been dominantly focused on lymphocytes [26,31,32]. The PD-1/PD-L1 axis signaling is considered to be one of the primary mechanisms that result in T cell dysfunction and death [16,33]. Recently, the new discovery of cell-intrinsic PD-1 in melanoma, hepatocellular carcinoma, and NSCLC was reported, explaining its unique role in tumorigenesis. It was intriguing that the purpose of PD-1 in melanoma and hepatocellular carcinoma was opposite of that in NSCLC [17–19]. In melanoma and hepatocellular carcinoma, the mTOR signaling was upregulated by the tumor-intrinsic PD-1 and was established to be a key regulator of the pro-tumorigenic functions of tumor-intrinsic PD-1 [20]. However, our results showed that cell-intrinsic PD-1 in PDAC significantly facilitated tumor growth both in *vitro* and in *vivo* in line with previous reports in melanoma and hepatocellular carcinoma. As functional assays showed, PD-1 OE in cell lines significantly enhanced cell proliferation and inhibited apoptosis *in vitro*, and increased growth and tumor sizes in the xenograft model, while PD-1 KD showed the opposite results. All the *in vitro* and *in vivo* results support the theory that cell-intrinsic PD-1 performs an essential role in PDAC progression.

Through the RNA sequencing and LC-MS/MS data, Hippo signaling pathway was revealed as the central positive regulation in gene translation and cell fate. The Hippo-YAP signaling pathway is a kinase cascade leading from Mst1/2 to YAP and its paralog TAZ. YAP/TAZ is known as a candidate oncogene, while other components of the Hippo signaling pathway are tumor suppressor genes, whose dysregulations are observed in a variety of cancers. A great deal of research has

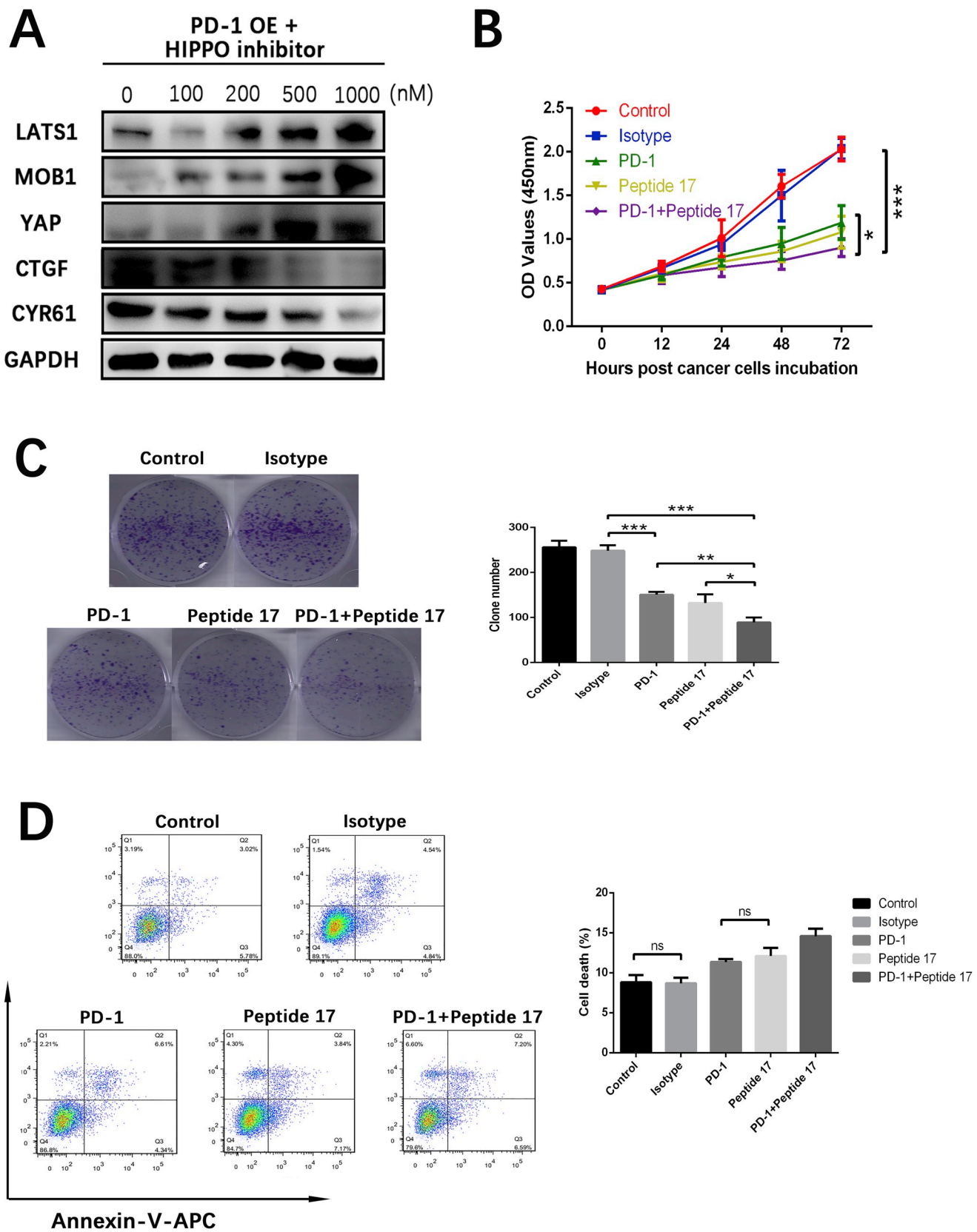

Fig. 5. PD-1 blockade in combination with a Hippo signaling inhibitor suppresses PDAC growth *in vitro*. (A) Western blot analysis of Hippo signaling pathway and down streams in the PD-1 overexpression (OE) MIA-PaCa-2 cells treated with different concentrations of Hippo inhibitors (Peptide 17). (B) CCK-8 assays at 0, 12, 24, 48, 72 h for cell proliferation after treatment of *anti*-PD-1 antibody and Hippo inhibitors (Peptide 17) for the PD-1 OE MIA-PaCa-2 cells. (C) Clone formation assays and analyses for 2 weeks after treatment of *anti*-PD-1 antibody and Hippo inhibitors (Peptide 17) for the PD-1 OE MIA-PaCa-2 cells. (D) Flow cytometry data and analyses showing cell apoptosis in the PD-1 OE MIA-PaCa-2 cells after 48-h treatment of *anti*-PD-1 antibody and Hippo inhibitors (Peptide 17), all p-value < 0.05 except ns. *, p-value < 0.05; **, p-value < 0.01; ***, p-value < 0.001.

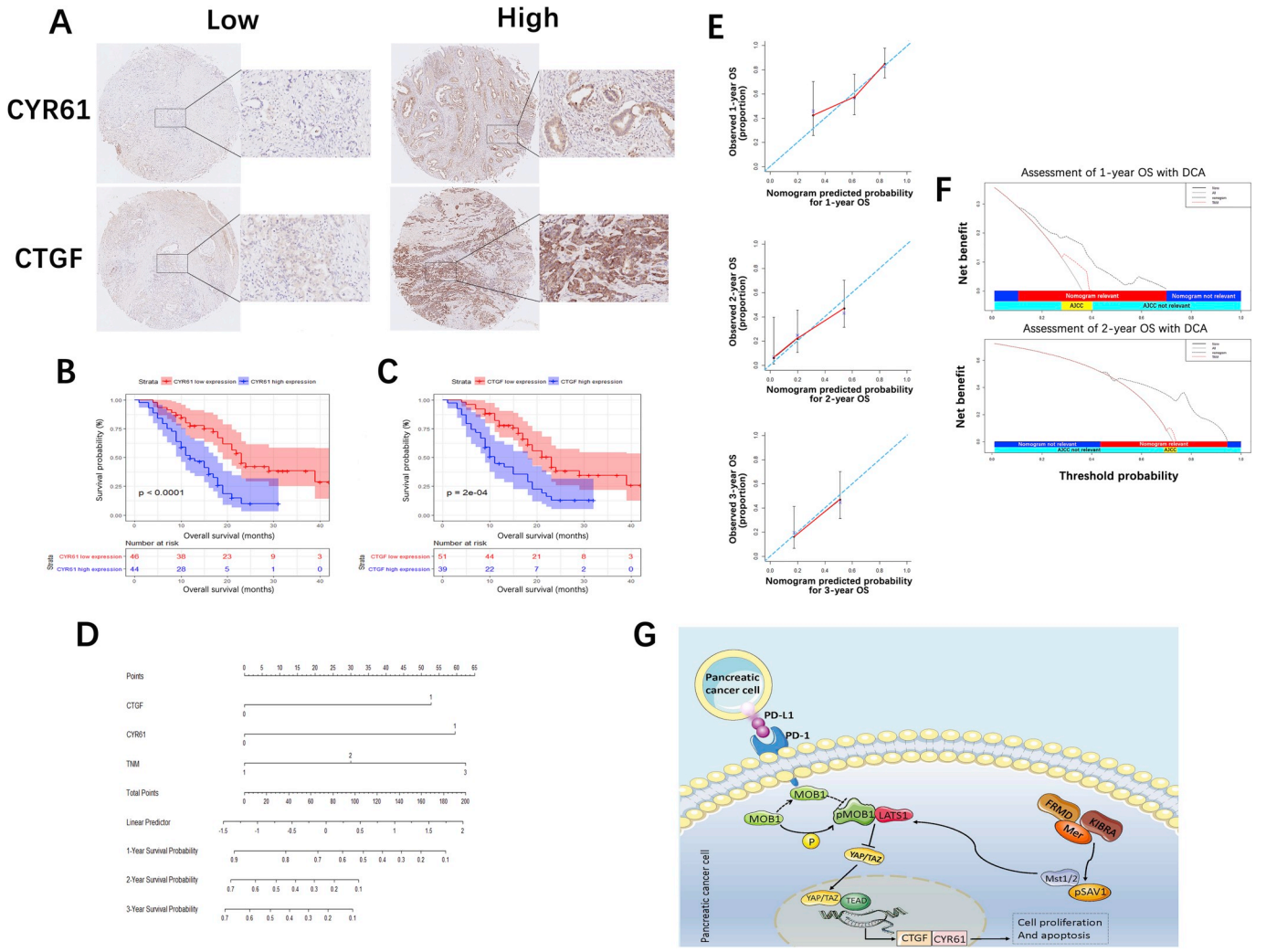

Fig. 6. Expression of CYR61/CTGF in PDAC tissue microarray and their predictive role in prognosis. (A) The representative images illustrating low and high expression of CYR61 and CTGF (× 40 low-power and × 400 high-power fields respectively). Kaplan–Meier survival curves of (B) CYR61 and (C) CTGF analyzed by Log-rank test. (D) The novel formulated nomogram containing CYR61, CTGF and AJCC 8th staging system. (E) The calibration curves depicting the observed and nomogram predicted overall survival at 1, 2 and 3 years. (F) The comparison of prognostic prediction between formulated nomogram model and AJCC 8th staging system by decision curve analysis. (G) The schematic drawing of PD-1 function in pancreatic cancer cell.

elucidated the features of Hippo signaling in tumorigenesis and progression and provided an abundant source of potential targets for cancer therapies [34–37]. Our results from IHC or IF staining and immunoprecipitation followed by western blotting further revealed that cell-intrinsic PD-1 might automatically bind to MOB1 and then decrease its phosphorylation. MOB1 is a central component of the Hippo signaling pathway, and pMOB1 undergoes conformational activation and binds to LATS1 [38,39]. Hergovich et al. [40] reported that down-regulation of LATS1 contributed to tumor formation in mammals. Notably, the interaction with MOB1 determined the tumor suppressor activity, and the mechanism of LATS1 activation typically depended on rapid recruitment to the plasma membrane by MOB1 followed by multisite phosphorylation. Our study showed that cell-intrinsic PD-1 bound to MOB1 and decreased its phosphorylation. Reduced pMOB1 suppressed LATS1 phosphorylation and then inactivated LATS1, which enabled the inhibition of YAP phosphorylation and the accumulation of YAP proteins. Then, the accumulated YAP proteins further combined with TEAD and translocated into the nucleus to activate the genes downstream of Hippo signaling pathway, such as CYR61 and CTGF expression (Fig. 6G).

We combined the *anti*-PD-1 and Peptide 17 treatment *in vitro*. Further functional assays showed that this combination treatment had a superior inhibitory impact on tumor growth than a single treatment. Hippo inhibitors were also identified as having a role in the tumor suppression of PDAC [41,42]. Downstream Hippo signaling targets contain CYR61 and CTGF, which commonly act as factors stimulating aggressiveness in a variety of cancers [21,23,43–45]. Haque et al. [22] reported that CYR61 expression was exorbitantly higher in cancer cells and significantly triggered the aggressive phenotype in PADC. Concomitantly, Bennewith et al. [24] also said that CTGF was a fibrosis-related gene related to pancreatic cancer progression. Mechanistically, CTGF protected pancreatic cancer cells from hypoxia-mediated apoptosis, and tumor cell-derived CTGF was vital for pancreatic cancer growth. Our results showed that cell-intrinsic PD-1 induced CYR61 and CTGF expression via the Hippo signaling pathway. In addition, TMA analysis of PDAC further revealed that CYR61 and CTGF were significantly associated with OS, and both indicators appeared to be independent prognostic factors.

According to the findings above, cell-intrinsic PD-1-induced CYR61 and CTGF via Hippo signaling played a critical role in tumorigenesis and prognostic predictors so that a new predictive model could be established. The AJCC 8th TNM staging system was considered a good model for risk stratification in PDAC patients, but more modifications or enrollments were explored to obtain a better predictive model

[2,46,47]. In our study, we tried to formulate a novel nomogram containing CYR61, CTGF, and AJCC 8th staging to predict OS in patients with resected PDAC. Surprisingly, such a nomogram logically improved the predictive performance and refined an excellent risk stratification regarding calibration, DCA and C-index. This model may efficiently serve as a robust prognostic tool in future clinical practice. However, a large-scale and multicenter study is still needed for further validation.

In conclusion, cell-intrinsic PD-1 in pancreatic cancer cells facilitates in tumor growth by Hippo signaling pathway independent of the immune system. The combination of *anti*-PD-1with Hippo inhibitors shows a superior inhibitory effect on tumor growth in *vitro*, which is essential to understanding the underlying mechanisms that may be effective to improve the prognosis of PDAC patients. Finally, regarding the specific role of CYR61 and CTGF, the formulated nomogram may provide a robust rational strategy in future risk stratification and survival prediction.

Conflicts of interest

There is no conflict of interest.

Conflicts of interest

The authors declare no conflicts of interest.

Funding

This work was funded by the National Natural Science Foundation of China (No. 81773068).

Authors' contributions

NP, SSG, JY, and WHL conceived and designed the experiments. NP, SSG, HLY, and JAL performed the experiments. YF, WCW, LZ, YFR, DSW, XFX, TTK, and DYJ acquired and analyzed the data. NP and JY wrote the manuscript. All authors read, edited and approved the final manuscript.

Acknowledgments

We thank the China Scholarship Council for supporting Dr. Pu as a visiting PhD candidate at Johns Hopkins University School of Medicine.

Abbreviations

PDAC	pancreatic ductal adenocarcinoma
OS	overall survival
TMA	tissue microarray
PD-1	programmed cell death protein-1
CYR61	cysteine-rich angiogenic inducer 61
CTGF	connective tissue growth factor
ICI	immune checkpoint inhibitor
NSCLC	nonsmall cell lung cancer
PD-L1	programmed death ligand 1
TCGA	the Cancer Genomic Atlas
CCLE	Cancer Cell Line Encyclopedia
MOB1	Mps1-One binder
DMEM	Dulbecco's Modified Eagle's Medium
qRT-PCR	quantitative real-time polymerase chain reaction
CCK-8	cell counting kit-8; PBS, phosphate buffer saline
YAP-TEAD	yes-associated protein-transcriptional enhanced associate domain
FCM	flow cytometry
MFI	mean fluorescence intensity
SDS-PAGE	sodium dodecyl sulfate-polyacrylamide gel electrophoresis
PVDF	polyvinylidene difluoride
IHC	immunohistochemistry
FFPE	formalin-fixed, paraffin-embedded
IF	immunofluorescence
LC-MS	liquid chromatography–mass spectrometry
HPLC	high performance liquid chromatography
HCD	high-energy collisional dissociation
pAGC	predictive Automatic Gain Control
SPF	specific pathogen free
OE	overexpressing
KD	knockdown
IPA	Ingenuity pathway analysis
LATS1	Large Tumor Suppressor homologue kinases 1
HPF	high-power field
DCA	decision curve analysis
HR	hazard ratio
CI	confidence interval

Appendix A. Supplementary data

Supplementary data to this article can be found online at https://doi.org/10.1016/j.canlet.2019.06.013.

References

[1] R.L. Siegel, K.D. Miller, A. Jemal, Cancer statistics, 2018, CA A Cancer J. Clin. 68 (2018) 7–30.
[2] N. Pu, S. Gao, Y. Xu, G. Zhao, Y. Lv, A. Nuerxiati, J.A. Li, D. Wang, X. Xu, T. Kuang, X. Wang, W. Lou, L. Liu, W. Wu, Alkaline phosphatase-to-albumin ratio as a prognostic indicator in pancreatic ductal adenocarcinoma after curative resection, J. Cancer 8 (2017) 3362–3370.
[3] O. Strobel, J. Neoptolemos, D. Jager, M.W. Buchler, Optimizing the outcomes of pancreatic cancer surgery, Nature reviews, Clin. Oncol. 16 (2019) 11–26.
[4] T.F. Greten, B. Sangro, Targets for immunotherapy of liver cancer, J. Hepatol. 68 (2018) 157–166.
[5] V.V. Subhash, M.S. Yeo, W.L. Tan, W.P. Yong, Strategies and advancements in harnessing the immune system for gastric cancer immunotherapy, J. Immunol. Res. 2015 (2015) 308574.
[6] K.Y. Elahi-Gedwillo, M. Carlson, J. Zettervall, P.P. Provenzano, Antifibrotic therapy disrupts stromal barriers and modulates the immune landscape in pancreatic ductal adenocarcinoma, Cancer Res. 79 (2019) 372–386.
[7] I.M. Stromnes, A. Hulbert, R.H. Pierce, P.D. Greenberg, S.R. Hingorani, T-cell localization, activation, and clonal expansion in human pancreatic ductal adenocarcinoma, Cancer Immunol. Res. 5 (2017) 978–991.
[8] P.P. Provenzano, C. Cuevas, A.E. Chang, V.K. Goel, D.D. Von Hoff, S.R. Hingorani, Enzymatic targeting of the stroma ablates physical barriers to treatment of pancreatic ductal adenocarcinoma, Cancer Cell 21 (2012) 418–429.
[9] K. Suresh, J. Naidoo, C.T. Lin, S. Danoff, Immune checkpoint immunotherapy for non-small cell lung cancer: benefits and pulmonary toxicities, Chest 154 (2018) 1416–1423.
[10] E.E. Rassy, R.M. Khoury Abboud, N. Ibrahim, T. Assi, F. Aoun, J. Kattan, The current state of immune checkpoint inhibitors in the first-line treatment of renal cancer, Immunotherapy 10 (2018) 1047–1052.
[11] R.N. Amaria, S.M. Reddy, H.A. Tawbi, M.A. Davies, M.I. Ross, I.C. Glitza, J.N. Cormier, C. Lewis, W.J. Hwu, E. Hanna, A. Diab, M.K. Wong, R. Royal, N. Gross, R. Weber, S.Y. Lai, R. Ehlers, J. Blando, D.R. Milton, S. Woodman, R. Kageyama, D.K. Wells, P. Hwu, S.P. Patel, A. Lucci, A. Hessel, J.E. Lee, J. Gershenwald, L. Simpson, E.M. Burton, L. Posada, L. Haydu, L. Wang, S. Zhang, A.J. Lazar, C.W. Hudgens, V. Gopalakrishnan, A. Reuben, M.C. Andrews, C.N. Spencer, V. Prieto, P. Sharma, J. Allison, M.T. Tetzlaff, J.A. Wargo, Neoadjuvant immune checkpoint blockade in high-risk resectable melanoma, Nat. Med. 24 (2018) 1649–1654.
[12] G. Chen, A.C. Huang, W. Zhang, G. Zhang, M. Wu, W. Xu, Z. Yu, J. Yang, B. Wang, H. Sun, H. Xia, Q. Man, W. Zhong, L.F. Antelo, B. Wu, X. Xiong, X. Liu, L. Guan, T. Li, S. Liu, R. Yang, Y. Lu, L. Dong, S. McGettigan, R. Somasundaram, R. Radhakrishnan, G. Mills, Y. Lu, J. Kim, Y.H. Chen, H. Dong, Y. Zhao, G.C. Karakousis, T.C. Mitchell, L.M. Schuchter, M. Herlyn, E.J. Wherry, X. Xu, W. Guo, Exosomal PD-L1 contributes to immunosuppression and is associated with anti-PD-1 response, Nature 560 (2018) 382–386.
[13] N. Pu, G. Zhao, H. Yin, J.A. Li, A. Nuerxiati, D. Wang, X. Xu, T. Kuang, D. Jin, W. Lou, W. Wu, CD25 and TGF-beta blockade based on predictive integrated immune ratio inhibits tumor growth in pancreatic cancer, J. Transl. Med. 16 (2018) 294.
[14] S.L. Topalian, J.M. Taube, R.A. Anders, D.M. Pardoll, Mechanism-driven biomarkers to guide immune checkpoint blockade in cancer therapy, Nature reviews, Cancer 16 (2016) 275–287.
[15] L. Zhang, T.F. Gajewski, J. Kline, PD-1/PD-L1 interactions inhibit antitumor immune responses in a murine acute myeloid leukemia model, Blood 114 (2009) 1545–1552.

[16] Z.Y. Xu-Monette, M. Zhang, J. Li, K.H. Young, PD-1/PD-L1 blockade: have we found the key to unleash the antitumor immune response? Front. Immunol. 8 (2017) 1597.
[17] S. Kleffel, C. Posch, S.R. Barthel, H. Mueller, C. Schlapbach, E. Guenova, C.P. Elco, N. Lee, V.R. Juneja, Q. Zhan, C.G. Lian, R. Thomi, W. Hoetzenecker, A. Cozzio, R. Dummer, M.C. Mihm Jr., K.T. Flaherty, M.H. Frank, G.F. Murphy, A.H. Sharpe, T.S. Kupper, T. Schatton, Melanoma cell-intrinsic PD-1 receptor functions promote tumor growth, Cell 162 (2015) 1242–1256.
[18] H. Li, X. Li, S. Liu, L. Guo, B. Zhang, J. Zhang, Q. Ye, Programmed cell death-1 (PD-1) checkpoint blockade in combination with a mammalian target of rapamycin inhibitor restrains hepatocellular carcinoma growth induced by hepatoma cell-intrinsic PD-1, Hepatology 66 (2017) 1920–1933.
[19] S. Du, N. McCall, K. Park, Q. Guan, P. Fontina, A. Ertel, T. Zhan, A.P. Dicker, B. Lu, Blockade of Tumor-Expressed PD-1 promotes lung cancer growth, OncoImmunology 7 (2018) e1408747.
[20] H. Yao, H. Wang, C. Li, J.Y. Fang, J. Xu, Cancer cell-intrinsic PD-1 and implications in combinatorial immunotherapy, Front. Immunol. 9 (2018) 1774.
[21] Y.L. Hsu, J.Y. Hung, S.H. Chou, M.S. Huang, M.J. Tsai, Y.S. Lin, S.Y. Chiang, Y.W. Ho, C.Y. Wu, P.L. Kuo, Angiomotin decreases lung cancer progression by sequestering oncogenic YAP/TAZ and decreasing Cyr61 expression, Oncogene 34 (2015) 4056–4068.
[22] I. Haque, S. Mehta, M. Majumder, K. Dhar, A. De, D. McGregor, P.J. Van Veldhuizen, S.K. Banerjee, S. Banerjee, Cyr61/CCN1 signaling is critical for epithelial-mesenchymal transition and stemness and promotes pancreatic carcinogenesis, Mol. Cancer 10 (2011) 8.
[23] C.R. Goodwin, B. Lal, X. Zhou, S. Ho, S. Xia, A. Taeger, J. Murray, J. Laterra, Cyr61 mediates hepatocyte growth factor-dependent tumor cell growth, migration, and Akt activation, Cancer Res. 70 (2010) 2932–2941.
[24] K.L. Bennewith, X. Huang, C.M. Ham, E.E. Graves, J.T. Erler, N. Kambham, J. Feazell, G.P. Yang, A. Koong, A.J. Giaccia, The role of tumor cell-derived connective tissue growth factor (CTGF/CCN2) in pancreatic tumor growth, Cancer Res. 69 (2009) 775–784.
[25] A.J. Vickers, E.B. Elkin, Decision curve analysis: a novel method for evaluating prediction models, Med. Decis. Mak. 26 (2006) 565–574.
[26] S.L. Topalian, C.G. Drake, D.M. Pardoll, Targeting the PD-1/B7-H1(PD-L1) pathway to activate anti-tumor immunity, Curr. Opin. Immunol. 24 (2012) 207–212.
[27] L. Zheng, PD-L1 expression in pancreatic cancer, J. Natl. Cancer Inst. 109 (2017) djw304.
[28] T. Nomi, M. Sho, T. Akahori, K. Hamada, A. Kubo, H. Kanehiro, S. Nakamura, K. Enomoto, H. Yagita, M. Azuma, Y. Nakajima, Clinical significance and therapeutic potential of the programmed death-1 ligand/programmed death-1 pathway in human pancreatic cancer, Clin. Cancer Res. 13 (2007) 2151–2157.
[29] T.A. Mace, R. Shakya, J.R. Pitarresi, B. Swanson, C.W. McQuinn, S. Loftus, E. Nordquist, Z. Cruz-Monserrate, L. Yu, G. Young, X. Zhong, T.A. Zimmers, M.C. Ostrowski, T. Ludwig, M. Bloomston, T. Bekaii-Saab, G.B. Lesinski, IL-6 and PD-L1 antibody blockade combination therapy reduces tumour progression in murine models of pancreatic cancer, Gut 67 (2018) 320–332.
[30] C. Feig, J.O. Jones, M. Kraman, R.J. Wells, A. Deonarine, D.S. Chan, C.M. Connell, E.W. Roberts, Q. Zhao, O.L. Caballero, S.A. Teichmann, T. Janowitz, D.I. Jodrell, D.A. Tuveson, D.T. Fearon, Targeting CXCL12 from FAP-expressing carcinoma-associated fibroblasts synergizes with anti-PD-L1 immunotherapy in pancreatic cancer, Proc. Natl. Acad. Sci. U. S. A. 110 (2013) 20212–20217.
[31] Z. Wang, E.G. Aguilar, J.I. Luna, C. Dunai, L.T. Khuat, C.T. Le, A. Mirsoian, C.M. Minnar, K.M. Stoffel, I.R. Sturgill, S.K. Grossenbacher, S.S. Withers, R.B. Rebhun, D.J. Hartigan-O'Connor, G. Mendez-Lagares, A.F. Tarantal, R.R. Isseroff, T.S. Griffith, K.A. Schalper, A. Merleev, A. Saha, E. Maverakis, K. Kelly, R. Aljumaily, S. Ibrahimi, S. Mukherjee, M. Machiorlatti, S.K. Vesely, D.L. Longo, B.R. Blazar, R.J. Canter, W.J. Murphy, A.M. Monjazeb, Paradoxical effects of obesity on T cell function during tumor progression and PD-1 checkpoint blockade, Nat. Med. 25 (2019) 141–151.
[32] E. Gianchecchi, A. Fierabracci, Inhibitory receptors and pathways of lymphocytes: the role of PD-1 in treg development and their involvement in autoimmunity onset and cancer progression, Front. Immunol. 9 (2018) 2374.
[33] C. Blank, T.F. Gajewski, A. Mackensen, Interaction of PD-L1 on tumor cells with PD-1 on tumor-specific T cells as a mechanism of immune evasion: implications for tumor immunotherapy, Cancer Immunol. Immunother. 54 (2005) 307–314.
[34] Y. Ma, Y. Yang, F. Wang, Q. Wei, H. Qin, Hippo-YAP signaling pathway: a new paradigm for cancer therapy, Int. J. Cancer 137 (2015) 2275–2286.
[35] C.G. Hansen, Y.L. Ng, W.L. Lam, S.W. Plouffe, K.L. Guan, The Hippo pathway effectors YAP and TAZ promote cell growth by modulating amino acid signaling to mTORC1, Cell Res. 25 (2015) 1299–1313.
[36] A.M. Tremblay, E. Missiaglia, G.G. Galli, S. Hettmer, R. Urcia, M. Carrara, R.N. Judson, K. Thway, G. Nadal, J.L. Selfe, G. Murray, R.A. Calogero, C. De Bari, P.S. Zammit, M. Delorenzi, A.J. Wagers, J. Shipley, H. Wackerhage, F.D. Camargo, The Hippo transducer YAP1 transforms activated satellite cells and is a potent effector of embryonal rhabdomyosarcoma formation, Cancer Cell 26 (2014) 273–287.
[37] M. Gomez, V. Gomez, A. Hergovich, The Hippo pathway in disease and therapy: cancer and beyond, Clin. Transl. Med. 3 (2014) 22.
[38] K. Otsubo, H. Goto, M. Nishio, K. Kawamura, S. Yanagi, W. Nishie, T. Sasaki, T. Maehama, H. Nishina, K. Mimori, T. Nakano, H. Shimizu, T.W. Mak, K. Nakao, Y. Nakanishi, A. Suzuki, MOB1-YAP1/TAZ-NKX2.1 axis controls bronchioalveolar cell differentiation, adhesion and tumour formation, Oncogene 36 (2017) 4201–4211.
[39] L. Ni, Y. Zheng, M. Hara, D. Pan, X. Luo, Structural basis for Mob1-dependent activation of the core Mst-Lats kinase cascade in Hippo signaling, Genes Dev. 29 (2015) 1416–1431.
[40] A. Hergovich, D. Schmitz, B.A. Hemmings, The human tumour suppressor LATS1 is activated by human MOB1 at the membrane, Biochem. Biophys. Res. Commun. 345 (2006) 50–58.
[41] Y. Liu, J. Lu, Z. Zhang, L. Zhu, S. Dong, G. Guo, R. Li, Y. Nan, K. Yu, Y. Zhong, Q. Huang, Amlexanox, a selective inhibitor of IKBKE, generates anti-tumoral effects by disrupting the Hippo pathway in human glioblastoma cell lines, Cell Death Dis. 8 (2017) e3022.
[42] F. Gibault, F. Bailly, M. Corvaisier, M. Coevoet, G. Huet, P. Melnyk, P. Cotelle, Molecular features of the YAP inhibitor verteporfin: synthesis of hexasubstituted dipyrrins as potential inhibitors of YAP/TAZ, the downstream effectors of the hippo pathway, ChemMedChem 12 (2017) 954–961.
[43] Y. Makino, H. Hikita, T. Kodama, M. Shigekawa, R. Yamada, R. Sakamori, H. Eguchi, E. Morii, H. Yokoi, M. Mukoyama, S. Hiroshi, T. Tatsumi, T. Takehara, CTGF mediates tumor-stroma interactions between hepatoma cells and hepatic stellate cells to accelerate HCC progression, Cancer Res. 78 (2018) 4902–4914.
[44] D. Xie, D. Yin, H.J. Wang, G.T. Liu, R. Elashoff, K. Black, H.P. Koeffler, Levels of expression of CYR61 and CTGF are prognostic for tumor progression and survival of individuals with gliomas, Clin. Cancer Res. 10 (2004) 2072–2081.
[45] F. Tanaka, A. Rizqiawan, K. Higashikawa, K. Tobiume, G. Okui, H. Shigeishi, S. Ono, H. Shimasue, N. Kamata, Snail promotes Cyr61 secretion to prime collective cell migration and form invasive tumor nests in squamous cell carcinoma, Cancer Lett. 329 (2013) 243–252.
[46] N. Pu, J. Li, Y. Xu, W. Lee, Y. Fang, X. Han, G. Zhao, L. Zhang, A. Nuerxiati, H. Yin, W. Wu, W. Lou, Comparison of prognostic prediction between nomogram based on lymph node ratio and AJCC 8th staging system for patients with resected pancreatic head carcinoma: a SEER analysis, Cancer Manag. Res. 10 (2018) 227–238.
[47] C.R. Ferrone, M.W. Kattan, J.S. Tomlinson, S.P. Thayer, M.F. Brennan, A.L. Warshaw, Validation of a postresection pancreatic adenocarcinoma nomogram for disease-specific survival, J. Clin. Oncol. 23 (2005) 7529–7535.